Article

Snow Surface Albedo Sensitivity to Black Carbon: Radiative Transfer Modelling

Nicholas D. Beres [1,2,*] [ID], **Magín Lapuerta** [3] [ID], **Francisco Cereceda-Balic** [4,5] and
Hans Moosmüller [2] [ID]

1   Faculty of Physics, University of Vienna, 1090 Vienna, Austria
2   Laboratory for Aerosol Science, Spectroscopy, and Optics, Desert Research Institute, Reno, NV 89512, USA; Hans.Moosmuller@dri.edu
3   Escuela Técnica Superior de Ingenieros Industriales. Universidad de Castilla-La Mancha, 13071 Ciudad Real, Spain; Magin.Lapuerta@uclm.es
4   Centre for Environmental Technologies, Universidad Técnica Federico Santa María, Valparaíso 2340000, Chile; francisco.cereceda@usm.cl
5   Department of Chemistry, Universidad Técnica Federico Santa María, Valparaíso 2340000, Chile
*   Correspondence: nicholas.beres@univie.ac.at

check for
updates

Abstract: The broadband surface albedo of snow can greatly be reduced by the deposition of light-absorbing impurities, such as black carbon on or near its surface. Such a reduction increases the absorption of solar radiation and may initiate or accelerate snowmelt and snow albedo feedback. Coincident measurements of both black carbon concentration and broadband snow albedo may be difficult to obtain in field studies; however, using the relationship developed in this simple model sensitivity study, black carbon mass densities deposited can be estimated from changes in measured broadband snow albedo, and vice versa. Here, the relationship between the areal mass density of black carbon found near the snow surface to the amount of albedo reduction was investigated using the popular snow radiative transfer model Snow, Ice, and Aerosol Radiation (SNICAR). We found this relationship to be linear for realistic amounts of black carbon mass concentrations, such as those found in snow at remote locations. We applied this relationship to measurements of broadband albedo in the Chilean Andes to estimate how vehicular emissions contributed to black carbon (BC) deposition that was previously unquantified.

Keywords: snow albedo; black carbon; radiative transfer modelling

1. Introduction

Uncontaminated snow surfaces are among the whitest natural surfaces encountered on Earth with one of the highest broadband albedos in the solar spectrum. However, in addition to the properties of snow and ice itself (such as ice grain size [1,2] and shape [3,4], surface roughness [5], and thickness of the snowpack [4]), contamination due to the deposition of light-absorbing impurities such as black carbon (BC) particles [6], the dominant light-absorbing aerosol in the atmosphere [7,8], can drastically reduce snow surface albedo [9–11] and increase the absorption of solar radiation, leading to accelerated snowmelt and snow albedo feedback [12–14]. The Snow, Ice, and Aerosol Radiation (SNICAR) model [12] describes scattering and absorption by snow and impurity mixtures with Mie theory [4,15] and uses a two-stream, multi-layer radiative transfer solution [16] to represent vertical inhomogeneities of the snow. Here, we use SNICAR to investigate relationships between snow surface albedo reduction and BC mass density deposited near the surface of an otherwise uncontaminated semi-infinite snowpack to show that unknown amounts of BC mass can be estimated from measurements of the broadband snow albedo, and vice versa.
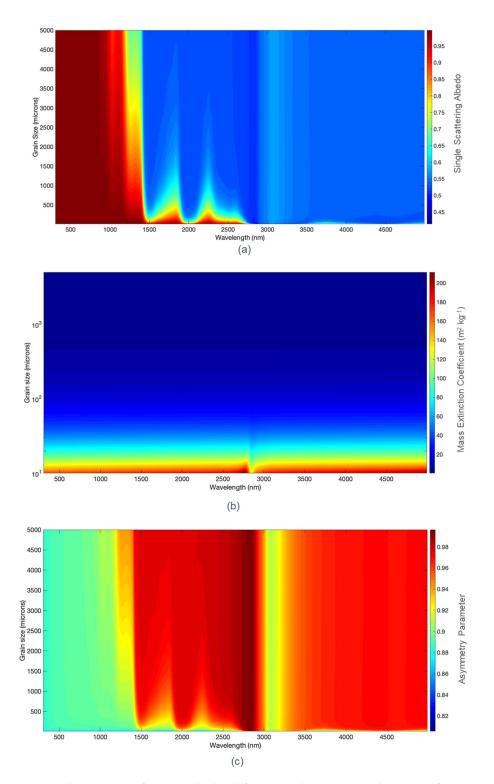
This study was motivated by recent observational work at Portillo, in the Chilean Andes [17], that quantified snow albedo reductions due to the deposition of unquantified amounts of BC from vehicle emission near the top of the snowpack; our work uses these albedo reductions to assess the corresponding areal BC mass density deposited to better understand the impact of anthropogenic activities on the South American cryosphere.

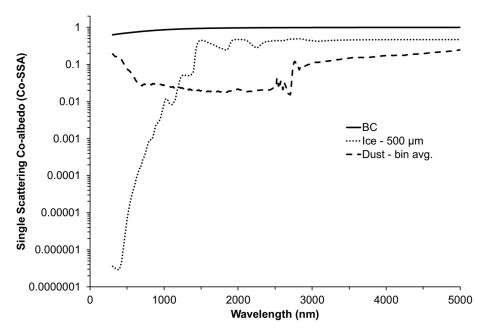## 2. Snow, Ice, and Aerosol Radiation (SNICAR) Model and Code

SNICAR is a radiative transfer model that couples irradiance with aerosol and snowpack optics including multiple scattering approximations to quickly and accurately estimate broadband snow albedo or spectral hemispherical snow albedo. It is parameterized through default and customizable user inputs of sky conditions (spectral direct or diffuse incident radiation, solar zenith angle, incident spectral radiance profile), snowpack properties (layer thickness, grain effective radius, mass density, underlying surface albedo), and aerosol characteristics (type and mass mixing ratio). All of the input parameters can be modified to suit the user's needs, such as defining a non-default surface spectral irradiance, redefining the optical properties of ice (e.g., Singh and Flanner [18]), or adding optical properties for custom impurities—such as brown carbon [19] and snow algae [20]. Standalone SNICAR code is available for multi-layer simulations as MATLAB (The MathWorks, Inc., Natick, MA, USA) code or as a web-based, single-layer simulator (both available from http://snow.engin.umich.edu). A previous, well-distributed version of the model outputs spectral quantities of interest in 470 spectral bands spanning 300–5000 nm at a 10 nm resolution; a newer, more comprehensive version of the SNICAR model was recently developed to address some limitations in the original code. This study uses the former, earlier iteration of the offline version of SNICAR.

The optical properties (mass extinction coefficient (MEC, m^2/kg), asymmetry parameter (g), and single scattering albedo (SSA)) of ice and impurities are computed offline using Mie theory [21] and collected as lookup tables for inputs necessary to the two-stream approximations. For ice, optical properties for effective radii from 10 to 5000 μm (increments of 1 μm between 10 and 1500 μm together with values of 2000, 3000, 4000, and 5000 μm) across the full SNICAR spectrum (i.e., 300–5000 nm) are calculated using optical constants from Warren and Brandt [22]; an overview of these properties is shown in Figure 1 as a function of ice effective grain radii. For BC, SNICAR uses an uncoated, hydrophobic black carbon model, where the refractive index spectrum is derived from Chang and Charalampopoulos [23]. Particle size and shape have been shown to be an important factor in estimating BC's effect on snow optical properties [24,25]; in SNICAR, the optical properties of BC are calculated using a log-normal size distribution with a number-median diameter of 100 nm and a geometric standard deviation of 1.5. Following the two-stream approach of Toon et al. [16], optical depths of snow and impurities are calculated and combined before the delta-Eddington approximation [26] is applied. While the model has been shown to effectively estimate snow surface albedo, some limitations apply, including assuming sphericity for ice and impurity particles as well as the mixing state of aerosol and ice (internal versus external) in the model [27]; some of these limitations and assumptions have been addressed in new versions of SNICAR.

Figure 1. Optical properties of ice, as calculated from Mie theory, across the range of wavelengths (300–5000 nm) and effective grain radii (10–5000 μm) available in Snow, Ice, and Aerosol Radiation (SNICAR). (**a**) The single-scattering albedo is near unity across all grain radii in the visible and near-visible wavelength range. (**b**) The mass extinction coefficient is nearly uniform over most of the wavelength and effective grain radius range. Note that the vertical axis uses a log-scale to highlight changes in MEC for small grain radii (<100 μm). (**c**) The large asymmetry parameter, g ($\approx$1), indicates mostly forward scattering across all wavelengths and effective grain radii, as expected for sizes much larger than the wavelength.

The effects of BC and other light-absorbing impurities on the snow albedo are most important in the near-UV, visible, and near-IR spectral range because ice itself is weakly absorbing in this range [15]. This is demonstrated if we examine the single-scattering co-albedo (co-SSA). If the SSA is the fraction of optical power that is scattered out of a beam incident on a particle, then the single scattering co-albedo (co-SSA = 1 − SSA) is the fraction of optical power removed from the incident beam due to particle absorption. For ice, this can be orders of magnitude lower than that of BC in the near-UV, visible, and near-IR wavelength regions, which is evident in Figure 2 comparing the co-SSA for ice, soot, and mineral dust calculated using default optical parameters in SNICAR. This large discrepancy illustrates that small concentrations of strongly absorbing impurities can greatly reduce snow albedo. For this study, we have addressed broadband albedo over the entire spectrum used in the model. However, we note that the spectral region above a wavelength of ~2.5 μm contributes very little to the broadband snow albedo due to near-zero solar irradiance within this region.

Figure 2. Single-scattering co-albedo (co-SSA = 1 − SSA) spectrum highlights the large discrepancy in the near-UV, visible, and near-IR wavelength regions (up to five to seven orders of magnitude) between the co-SSA of impurities, such as black carbon (BC) and mineral dust, compared to that of ice grains with a radius of 500 μm as used within the SNICAR model. Optical properties of BC were calculated using Mie theory with a number-mean diameter of 100 nm and a geometric standard deviation of 1.5. The co-SSA for dust has been averaged across all four size distributions available in SNICAR.
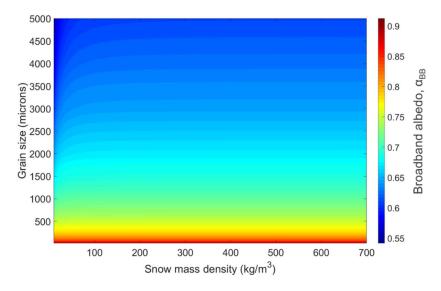
BC concentrations in the Sierra Nevada (Western U.S.) snowpack are generally low but are still sufficient to reduce snow albedo. Measured values of BC found in the snowpack can be on the order of hundreds ppb (ng BC/g). Sterle et al. [28] found mean amounts of BC concentration in the top 2 cm of the snowpack between ~25 ppb and ~135 ppb at the Mammoth Mountain Ski Resort, CA, during the 2009 accumulation and ablation season and found a gradual increase in BC concentration as the snowpack receded during the winter-spring seasonal transition. Similarly, in the Chilean Andes, the late season snowpack also allows insoluble light-absorbing impurities, including BC, to accumulate at the surface, as shown in Cereceda-Balic et al. [17]. These BC concentrations can have a significant impact to measured albedo, which can critically alter the Andean cryosphere [29] and its function as water reservoir for the region [30]. These previous studies motivated our investigation of the relationship between black carbon in snow and the resulting albedo reduction. For this, we focus on using SNICAR for the calculations of snow surface albedo for simple, yet representative snowpacks, as described in Section 3.

3. SNICAR Calculations of Broadband Snow Surface Albedo Sensitivity to Black Carbon (BC) Surface Deposition

Within SNICAR, we designed a semi-infinite snowpack of 10 m of depth with impurities relegated to the top-most 2 cm, representing surface deposition onto an otherwise clean snowpack, where these impurities impart the largest contribution to changes in surface snow albedo [31,32]. Note that such a semi-infinite snowpack is a good approximate for a snowpack thicker than the euphotic depth, which in winter is commonly around 10 cm but in spring can increase to about 50 cm [33]. We prescribe an effective grain radius of 250 μm and a snow mass density of 300 kg/m^3 as our "standard" snowpack for both the underlying 9.98-m-thick layer and for the top 0.02-m-thick layer. These values fall within the range of those found within maritime snowpacks [34] and are appropriate and representative of a midseason snowpack found in the Sierra Nevada or parts of the Chilean Andes. The BC areal mass density (*BCMD*), here defined as:

$$BCMD \left[\frac{mg\ BC}{m^2}\right] = BC \left[\frac{mg\ BC}{g}\right] \times Snow\ mass\ density \left[\frac{g}{m^3}\right] \times Thickness\ of\ BC\ layer[m], \quad (1)$$

reduces the complexity of the problem by including one of the other input parameters for the model, the snow mass density. For a semi-infinite snowpack, broadband albedo is largely independent of snow mass density [4,35], and, according to Figure 3, changes in SNICAR-derived broadband snow albedo as a function of snow mass density are noticeable only for very small snow densities and/or very large ice grain effective radii, otherwise contour lines are mostly horizontal.

Figure 3. Broadband snow surface albedo α_{BB} as a function of both snow grain radius and snow mass density calculated with the SNICAR model. α_{BB} is largely insensitive to changes in snow density for snow densities greater than ~100 kg/m^3 and grain radii smaller than ~2000 μm.

We used SNICAR to calculate broadband surface albedo α_{BB} as function of *BCMD*. The results (Figure 4) show how broadband snow surface albedo decreases as a function of *BCMD* deposited. The broadband snow surface albedo α_{BB}, as a function of the *BCMD* shown in Figure 4, can be described with less than 1.2% error by a cubic polynomial written as:

$$\alpha_{BB}(BCMD) = 0.777382 - \Delta\alpha_{BB}(BCMD) = 0.777382 \pm 0.001625 - [(0.017776\tfrac{m^2}{mg} \pm$$

$$0.000356\tfrac{m^2}{mg})\ BCMD] + \left[\left(0.000469\tfrac{m^2}{mg} \pm 0.000021\tfrac{m^2}{mg}\right) BCMD\right]^2 - [(0.000052\tfrac{m^2}{mg} \pm \quad (2)$$

$$0.000003\tfrac{m^2}{mg})\ BCMD]^3,$$

for $BCMD \leq 40$ mg/m^2. Here, $\Delta\alpha_{BB}(BCMD)$ is defined as the reduction of the broadband snow surface albedo of a pure snowpack $\alpha_{BB}(BCMD = 0)$ due to the addition of $BCMD$ to its top 0.02-m layer with:

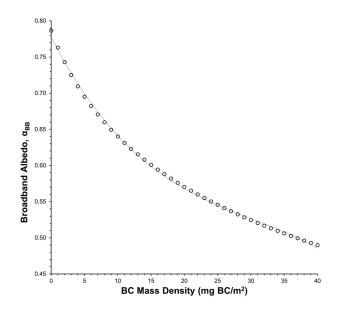$$\Delta\alpha_{BB}(BCMD) = \alpha_{BB}(0) - \alpha_{BB}(BCMD). \tag{3}$$

However, for a smaller $BCMD$ (i.e., $BCMD \leq 3$ mg/m^2), such as that encountered in most natural snowpacks [28,36], this relationship becomes near-linear and the reduction of surface albedo $\Delta\alpha_{BB}(BCMD)$ can be approximated by:

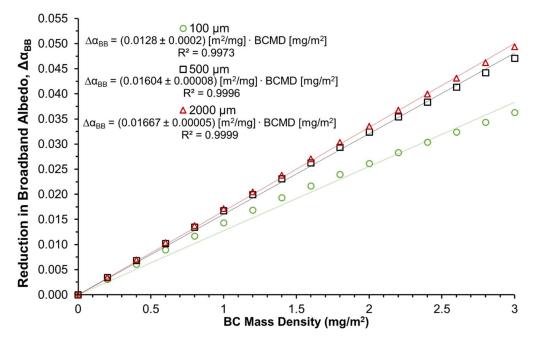$$\Delta\alpha_{BB}(BCMD) = m\left[\frac{m^2}{mg}\right] BCMD\left[\frac{mg}{m^2}\right], \tag{4}$$

where a single number, the slope m, characterizes the change in snow surface albedo per $BCMD$ added. Figure 5 shows the reduction of surface albedo $\Delta\alpha_{BB}$ as function of $BCMD$ for three grain radii (i.e., 100, 500, and 2000 µm) and the resulting linear regression slopes m for $BCMD \leq 3$ mg/m^2. Note that there is some dependence of linearity on ice effective grain radius, especially for small (i.e., 100 µm) values. Figure 6 shows calculated values for m as a function of grain radius for our "standard" snowpack in the range $0 \leq BCMD \leq 3$ mg/m^2 and indicates that, for grain radii between 500 and 5000 µm, the slope m is nearly constant (0.0161 m^2/mg $\leq m \leq$ 0.0167 m^2/mg). In addition, the initial slope m_0, for very low BCMD, defined as

$$m_0 = \lim_{BCMD\to0} m = 0.0173 \pm 0.0003 \frac{m^2}{mg} \tag{5}$$
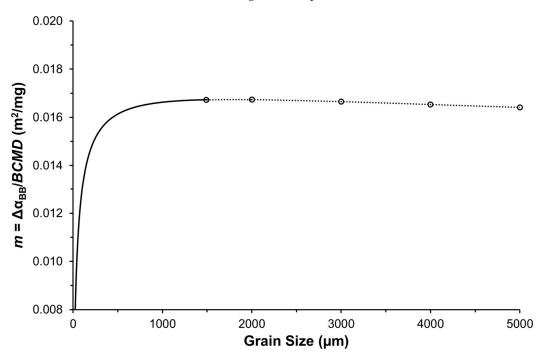
is nearly independent of grain radius for typically encountered effective grain radii between 100 and 2000 µm. The uncertainty is further reduced when we consider the average value of $m_0 = 0.0166 \pm 0.0002$ m^2/mg for more mature snowpacks with a grain radius between 500 and 5000 µm. In summary, the linear relationship of broadband snow surface albedo on $BCMD$ (Equation (4)) gives us a simple way, fairly independent of grain size, to estimate $BCMD$ from measured albedo changes or estimate (in reverse) broadband albedo changes from measured or modelled BC deposition.

Figure 4. Broadband snow surface albedo α_{BB} calculated with SNICAR (open circles for our standard snowpack) as a function of BC mass density ($BCMD$). The deposited BC aerosol is distributed uniformly in the top 2 cm of our 300 kg/m^3 "standard" snowpack. For example, using Equation (1), $BCMD$ of 40 mg BC/m^2 corresponds to a BC concentration of approximately 6700 ppb distributed in the top 2 cm. The solid line gives a cubic polynomial fit (Equation (2)) in good agreement (<1.2% error) with the SNICAR results.

Figure 5. Reduction of snow surface albedo $\Delta\alpha_{BB}$ as function of *BCMD* for three grain radii (i.e., 100, 500, and 2000 μm) and the resulting slopes *m* for *BCMD* $\leq$ 3 mg/m² from a linear regression, where the error of *m* is the standard error value of the regression slope.

Figure 6. Slope *m* as a function of grain radius for 0 mg/m² $\leq$ *BCMD* $\leq$ 3 mg/m². The grain radius resolution is 1 μm for the range 10–1500 μm and the values of *m* are shown as a continuous line, whereas the more discrete calculations of *m* for grain radii of 1500, 2000, 3000, 4000, and 5000 μm are shown as open circles interpolated with a dotted line.

4. Discussion

We can use Equations (4) and (5) to estimate BC deposition rates from measured changes in broadband snow albedo. For instance, Cereceda-Balic et al. [17] observed, for example, a one-day average reduction of broadband snow surface albedo $\Delta\alpha_{BB} = 0.08$ due to the deposition of BC from

~2000 vehicles passing by their albedo measurement site in the Chilean Andes. We approximate their one-day accumulated BC loading using a value of $m = 0.0166$ m^2/mg. Thus, according to Equation (4), this corresponds to a BC deposition rate of 4.8 mg/(m^2 day), which is the equivalent to an average BC deposition rate of 2.4 μg/m^2 per vehicle passing by.

These simple results are valuable to estimate the impacts of vehicular, industrial, and urban BC pollution on snow albedo due to BC deposition [37], or to estimate the extent to which BC aerosol deposition reduces broadband albedo and promotes early melting of snow and ice [38]. The verification of these methods is left for upcoming studies, wherein other methods (such as those outlined by Cereceda-Balic et al. [39,40]) to investigate BC-albedo feedbacks can be co-investigated with modeling and sensitivity studies similar to the investigation outlined here.

5. Conclusions

Here, we analyzed the decrease in broadband snow albedo as a function of BC mass deposited and obtain a simple model-based sensitivity for this relationship. Our findings suggest that, for real-world mass concentrations of BC deposited onto the snow surface, reductions in broadband albedo are directly proportional to the BC areal mass density and a slope parameter $m = 0.0166 \pm 0.0002$ m^2/mg, for grain radii between 500 and 5000 μm. Likewise, estimates of the reduction of broadband albedo can be performed using this same relationship when the deposited BC mass density is known. This relationship was used to estimate BC mass deposition from vehicular emissions in the Andes mountains.

Conflicts of Interest: The authors declare no conflict of interest.

References

1. Dang, C.; Fu, Q.; Warren, S.G. Effect of Snow Grain Shape on Snow Albedo. *J. Atmos. Sci.* **2016**, *73*, 3573–3583. [CrossRef]
2. Libois, Q.; Picard, G.; France, J.L.; Arnaud, L.; Dumont, M.; Carmagnola, C.M.; King, M.D. Influence of grain shape on light penetration in snow. *Cryosphere* **2013**, *7*, 1803–1818. [CrossRef]
3. Nolin, A.W.; Dozier, J. A Hyperspectral Method for Remotely Sensing the Grain Size of Snow. *Remote Sens. Environ.* **2000**, *74*, 207–216. [CrossRef]
4. Wiscombe, W.J.; Warren, S.G. A Model for the Spectral Albedo of Snow. I: Pure Snow. *J. Atmos. Sci.* **1980**, *37*, 2712–2733. [CrossRef]
5. Warren, S.G.; Brandt, R.E.; Hinton, P.O.R. Effect of surface roughness on bidirectional reflectance of Antarctic snow. *J. Geophys. Res. Space Phys.* **1998**, *103*, 25789–25807. [CrossRef]
6. Lack, D.A.; Moosmüller, H.; McMeeking, G.R.; Chakrabarty, R.K.; Baumgardner, D. Characterizing elemental, equivalent black, and refractory black carbon aerosol particles: A review of techniques, their limitations and uncertainties. *Anal. Bioanal. Chem.* **2014**, *406*, 99–122. [CrossRef] [PubMed]
7. Bond, T.C.; Doherty, S.J.; Fahey, D.W.; Forster, P.M.; Berntsen, T.; DeAngelo, B.J.; Flanner, M.G.; Ghan, S.; Kärcher, B.; Koch, D.; et al. Bounding the role of black carbon in the climate system: A scientific assessment. *J. Geophys. Res. Atmos.* **2013**, *118*, 5380–5552. [CrossRef]
8. Moosmüller, H.; Chakrabarty, R.K.; Arnott, W.P. Aerosol light absorption and its measurement: A review. *J. Quant. Spectrosc. Radiat. Transf.* **2009**, *110*, 844–878. [CrossRef]
9. Warren, S.G. Optical properties of snow. *Rev. Geophys.* **1982**, *20*, 67–89. [CrossRef]

10. Chýlek, P.; Ramaswamy, V.; Srivastava, V. Albedo of soot-contaminated snow. *J. Geophys. Res.* **1983**, *88*, 10837. [CrossRef]

11. Beres, N.D.; Moosmüller, H. Apparatus for dry deposition of aerosols on snow. *Atmos. Meas. Tech.* **2018**, *11*, 6803–6813. [CrossRef]

12. Flanner, M.G.; Zender, C.S.; Randerson, J.T.; Rasch, P.J. Present-day climate forcing and response from black carbon in snow. *J. Geophys. Res.* **2007**, *112*, D11202. [CrossRef]

13. Hansen, J.; Nazarenko, L. Soot climate forcing via snow and ice albedos. *Proc. Natl. Acad. Sci. USA* **2004**, *101*, 423–428. [CrossRef] [PubMed]

14. Skiles, S.M.; Flanner, M.; Cook, J.M.; Dumont, M.; Painter, T.H. Radiative forcing by light-absorbing particles in snow. *Nat. Clim. Chang.* **2018**, *8*, 964–971. [CrossRef]

15. Warren, S.G.; Wiscombe, W.J. A Model for the Spectral Albedo of Snow. II: Snow Containing Atmospheric Aerosols. *J. Atmos. Sci.* **1980**, *37*, 2734–2745. [CrossRef]

16. Toon, O.B.; McKay, C.P.; Ackerman, T.P.; Santhanam, K. Rapid calculation of radiative heating rates and photodissociation rates in inhomogeneous multiple scattering atmospheres. *J. Geophys. Res.* **1989**, *94*, 16287. [CrossRef]

17. Cereceda-Balic, F.; Vidal, V.; Moosmüller, H.; Lapuerta, M. Reduction of snow albedo from vehicle emissions at Portillo, Chile. *Cold Reg. Sci. Technol.* **2018**, *146*, 43–52. [CrossRef]

18. Singh, D.; Flanner, M.G. An improved carbon dioxide snow spectral albedo model: Application to Martian conditions. *J. Geophys. Res. Planets* **2016**, *121*, 2037–2054. [CrossRef]

19. Beres, N.D.; Sengupta, D.; Samburova, V.; Khlystov, A.Y.; Moosmüller, H. Deposition of brown carbon onto snow: Changes in snow optical and radiative properties. *Atmos. Chem. Phys.* **2020**, *20*, 6095–6114. [CrossRef]

20. Cook, J.M.; Hodson, A.J.; Gardner, A.S.; Flanner, M.; Tedstone, A.J.; Williamson, C.; Irvine-Fynn, T.D.L.; Nilsson, J.; Bryant, R.; Tranter, M. Quantifying bioalbedo: A new physically based model and discussion of empirical methods for characterising biological influence on ice and snow albedo. *Cryosphere* **2017**, *11*, 2611–2632. [CrossRef]

21. Mie, G. Beiträge zur Optik trüber Medien, speziell kolloidaler Metallösungen. *Ann. Phys.* **1908**, *330*, 377–445. [CrossRef]

22. Warren, S.G.; Brandt, R.E. Optical constants of ice from the ultraviolet to the microwave: A revised compilation. *J. Geophys. Res. Space Phys.* **2008**, *113*, 1–10. [CrossRef]

23. Chang, H.; Charalampopoulos, T.T. Determination of the wavelength dependence of refractive indices of flame soot. *Proc. R. Soc. Lond.* **1990**, *430*, 577–591. [CrossRef]

24. Schwarz, J.P.; Gao, R.S.; Perring, A.E.; Spackman, J.R.; Fahey, D.W. Black carbon aerosol size in snow. *Sci. Rep.* **2013**, *3*, 1–5. [CrossRef] [PubMed]

25. Liou, K.N.; Takano, Y.; Yang, P. Light absorption and scattering by aggregates: Application to black carbon and snow grains. *J. Quant. Spectrosc. Radiat. Transf.* **2011**, *112*, 1581–1594. [CrossRef]

26. Joseph, J.H.; Wiscombe, W.J.; Weinman, J.A. The Delta-Eddington Approximation for Radiative Flux Transfer. *J. Atmos. Sci.* **1976**, *33*, 2452–2459. [CrossRef]

27. He, C.; Flanner, M.G.; Chen, F.; Barlage, M.; Liou, K.N.; Kang, S.; Ming, J.; Qian, Y. Black carbon-induced snow albedo reduction over the Tibetan Plateau: Uncertainties from snow grain shape and aerosol-snow mixing state based on an updated SNICAR model. *Atmos. Chem. Phys.* **2018**, *18*, 11507–11527. [CrossRef]

28. Sterle, K.M.; McConnell, J.R.; Dozier, J.; Edwards, R.; Flanner, M.G. Retention and radiative forcing of black carbon in eastern Sierra Nevada snow. *Cryosphere* **2013**, *7*, 365–374. [CrossRef]

29. Rowe, P.M.; Cordero, R.R.; Warren, S.G.; Stewart, E.; Doherty, S.J.; Pankow, A.; Schrempf, M.; Casassa, G.; Carrasco, J.; Pizarro, J.; et al. Black carbon and other light-absorbing impurities in snow in the Chilean Andes. *Sci. Rep.* **2019**, *9*, 4008. [CrossRef]

30. Masiokas, M.H.; Villalba, R.; Luckman, B.H.; Le Quesne, C.; Aravena, J.C. Snowpack Variations in the Central Andes of Argentina and Chile, 1951–2005: Large-Scale Atmospheric Influences and Implications for Water Resources in the Region. *J. Clim.* **2006**, *19*, 6334–6352. [CrossRef]

31. Yasunari, T.J.; Tan, Q.; Lau, K.M.; Bonasoni, P.; Marinoni, A.; Laj, P.; Ménégoz, M.; Takemura, T.; Chin, M. Estimated range of black carbon dry deposition and the related snow albedo reduction over Himalayan glaciers during dry pre-monsoon periods. *Atmos. Environ.* **2013**, *78*, 259–267. [CrossRef]

32. Doherty, S.J.; Grenfell, T.C.; Forsström, S.; Hegg, D.L.; Brandt, R.E.; Warren, S.G. Observed vertical redistribution of black carbon and other insoluble light-absorbing particles in melting snow. *J. Geophys. Res. Atmos.* **2013**, *118*, 5553–5569. [CrossRef]

33. Zhong, E.; Li, Q.; Sun, S.; Chen, S.; Chen, W. Analysis of euphotic depth in snow with SNICAR transfer scheme. *Atmos. Sci. Lett.* **2017**, *18*, 484–490. [CrossRef]

34. Domine, F. Physical Properties of Snow. In *Encyclopedia of Snow, Ice and Glaciers*; Singh, V.P., Singh, P., Haritashya, U.K., Eds.; Springer: Berlin/Heidelberg, Germany, 2011; pp. 859–863. ISBN 978-90-481-2642-2.

35. Dozier, J.; Schneider, S.R.; McGinnis, D.F. Effect of grain size and snowpack water equivalence on visible and near-infrared satellite observations of snow. *Water Resour. Res.* **1981**, *17*, 1213–1221. [CrossRef]

36. Hadley, O.L.; Corrigan, C.E.; Kirchstetter, T.W.; Cliff, S.S.; Ramanathan, V. Measured black carbon deposition on the Sierra Nevada snow pack and implication for snow pack retreat. *Atmos. Chem. Phys.* **2010**, *10*, 7505–7513. [CrossRef]

37. Cereceda-Balic, F.; Palomo-Marín, M.R.; Bernalte, E.; Vidal, V.; Christie, J.; Fadic, X.; Guevara, J.L.; Miro, C.; Pinilla Gil, E. Impact of Santiago de Chile urban atmospheric pollution on anthropogenic trace elements enrichment in snow precipitation at Cerro Colorado, Central Andes. *Atmos. Environ.* **2012**, *47*, 51–57. [CrossRef]

38. Thind, P.S.; Chandel, K.K.; Sharma, S.K.; Mandal, T.K.; John, S. Light-absorbing impurities in snow of the Indian Western Himalayas: Impact on snow albedo, radiative forcing, and enhanced melting. *Environ. Sci. Pollut. Res.* **2019**, *6*, 7566–7578. [CrossRef]

39. Cereceda-Balic, F.; Vidal, V.; Ruggeri, M.F.; González, H.E. Black carbon pollution in snow and its impact on albedo near the Chilean stations on the Antarctic peninsula: First results. *Sci. Total Environ.* **2020**, *743*, 140801. [CrossRef]

40. Cereceda-Balic, F.; Gorena, T.; Soto, C.; Vidal, V.; Lapuerta, M.; Moosmüller, H. Optical determination of black carbon mass concentrations in snow samples: A new analytical method. *Sci. Total Environ.* **2019**, *697*, 133934. [CrossRef]